Shahid Beheshti University

Sustainable Earth Trends

Journal homepage: http://sustainearth.sbu.ac.ir

Monitoring air pollution using Sentinel-5 satellite imagery: A case study of Razavi and South Khorasan provinces

Fatemeh Kafi[a], Elham Yousefi[a,b*], Mohammad Ehteram[c], Khosro Ashrafi[d]

[a] Department of Environmental Engineering, Faculty of Natural Resources and Environment, University of Birjand, Birjand, Iran
[b] Research Group of Drought and Climate Change, University of Birjand, Birjand, Iran
[c] Department of Water Engineering, Faculty of Civil Engineering, Semnan University, Semnan, Iran
[d] Department of Environmental Engineering, Faculty of Environment, University of Tehran, Tehran, Iran

ABSTRACT

One of the significant challenges facing developing countries is combating air pollution and improving air quality. Therefore, analyzing changes in air pollutants can provide valuable information for experts to analyze air quality. The TROPOMI sensor on the Sentinel-5 satellite enables the tracking of gaseous pollutants. In this study, using GEE (Google Earth Engine), the products of CO, O_3, NO_2, and SO_2 pollutants were retrieved, and their average concentrations were mapped at the spatial scale of Razavi and South Khorasan provinces in the period 2018-2023. Additionally, the inverse distance weighting (IDW) method was used for annual data from five air quality monitoring stations. The results of this research showed that the spatial distribution of the concentration of these pollutants increased from Razavi and South Khorasan provinces, with the highest values recorded in the north, northeast, and center of Khorasan Razavi province. Also, the spatial distribution of the concentration of measured pollutants using the IDW model showed that the highest concentration dispersion of pollutants was recorded at the Mashin Abzar, Khiam, Sajad, and Tarog stations. To investigate the overall ability of the TRPOPMI sensor to estimate atmospheric pollutants, the coefficient of determination (R^2) was used. The results showed that the monitoring values using Sentinel-5 satellite images correlate at least 0.76% for CO, 0.85% for O_3, 0.79% for NO_2, and 0.78% for SO_2 with the values monitored by air quality monitoring stations.

ARTICLE INFO

Keywords:
Air pollutants
Google Earth Engine
IDW
TROPOMI sensor

Article history:
Received: 14 Sep 2024
Accepted: 01 Oct 2024

*Corresponding author
E-mail address:
e_yusefi_31@birjand.ac.ir
(E. Yousefi)

Citation:
Kafi, F. et al., (2024). Monitoring air pollution using Sentinel-5 satellite imagery: A case study of Razavi and South Khorasan provinces, *Sustainable Earth Trends:* 4(4), (41-55).

DOI: 10.48308/set.2024.236905.1067

1. Introduction

Air pollution is one of the most serious health threats today. This invisible killer claims the lives of many people annually. Numerous pollutants are present in the atmosphere, with ozone being one of the most dangerous, capable of causing severe health damage and premature mortality (Xiong et al., 2022). According to the World Health Organization, air pollution is a leading cause of premature death, accounting for approximately 4.2 million deaths globally each year due to lung cancer, heart disease, respiratory illnesses, and more. The rapid development of the economy, population growth, increasing industrialization, and growing transportation needs have all contributed to heightened environmental pollution, including air pollution (Juarez and Petersen, 2021).

Air pollutants originate from a combination of anthropogenic (vehicles, power plants, etc.) and biogenic (soil and vegetation) sources (Aljanabi et al., 2020). Nitrogen dioxide (NO_2), O_3, sulfur dioxide (SO_2), and carbon monoxide (CO) are key indicators of air pollution (Carbo-Bustinza et al., 2022). Primary air pollutants are emitted directly from a natural or human-made process, such as ash from a volcanic eruption, carbon monoxide gas from motor vehicle exhaust, or sulfur dioxide released from industries. Ground-level ozone as a major secondary pollutant, has been the subject of many studies in recent years (Wang et al., 2017; Maji et al., 2020; Ou et al., 2020; Zhao et al., 2021). Ozone is generated through chemical reactions of nitrogen oxides and volatile organic compounds in the presence

of favorable meteorological conditions, e.g., intense solar radiation, low humidity, high temperature, and low winds (Wang et al., 2017). Ozone concentration exhibits certain spatiotemporal changes and involves nonlinear, strong coupling and multivariate problems (Ezimand and Kakroodi, 2019; Su et al., 2020). In addition to emission sources, regional climate, and topography, which influence the transport, dispersion, and chemical transformations of pollutants, play a crucial role in air pollution (Tiwari et al., 2015). The following section provides a brief overview of some of the primary air pollutants examined in this paper.

Carbon monoxide is one of the most common and most poisonous air pollutants. Carbon monoxide is a hazardous gas mainly produced from the incomplete combustion of carbon. About two-thirds of carbon monoxide emissions are caused by human activities. Some of these include burning crop residues, fossil fuel combustion, and methane oxidation (Saxena and Naik, 2019). Due to its relatively short lifetime, carbon monoxide does not mix well in the troposphere. However, the emission of carbon monoxide into the atmosphere can affect the lifetime of methane and the production of tropospheric carbon dioxide and ozone, and therefore has a significant impact on global climate change (Ghandi et al., 2022).

Coal, oil, and several impure fuels contain sulfur as well as various organic compounds. The primary human source of sulfur dioxide emissions is the presence of sulfur in fossil fuels, which is released upon combustion. Relatively small amounts of sulfur are also released from wildfires, soils, and vegetation (Saxena and Naik, 2019). Large coal-fired power plants are the biggest sources of sulfur dioxide in the world, leading to the production of smog and acid rain, which in turn cause respiratory and lung diseases (Greenberg et al., 2016). Among the various pollutants in the atmosphere, nitrogen oxides are considered one of the most important pollutants and toxic gases (Dickerson et al., 2019; Park et al., 2021). Millions of tons of nitrogen dioxide and nitric oxide are produced annually due to human activities, especially the combustion of fossil fuels at high temperatures. Nitrogen dioxide, when combined with moist air, produces nitric acid, which causes severe corrosion of metals. Also, in high concentrations, it causes fog and significantly reduces visibility (Park et al., 2021). Nitrogen oxides are also known as "indirect greenhouse gases" because they enter the upper troposphere through lightning and play an important role in global warming by producing ozone (Grewe et al., 2012; Finney et al., 2016).

Ground-level ozone is a pollutant found near the Earth's surface (Pan et al., 2023). Unlike the protective ozone layer in the stratosphere that shields us from harmful ultraviolet radiation, ground-level ozone (henceforth referred to as ozone) can pose a threat to human health (Lingxia et al., 2023). Ozone can harm plants by reducing their ability to absorb sunlight and essential nutrients. It can also damage forests and other ecosystems (Cheng et al., 2023). Ozone production involves a complex series of chemical reactions. Nitrogen dioxide (NO_2) absorbs sunlight energy and breaks down into nitric oxide (NO) and an oxygen atom (Ehteram et al., 2023). Nitric oxide (NO) reacts with oxygen molecules (O_2) to form ozone (O_3). As ozone is a major air pollutant, accurate prediction and monitoring of its concentration is essential. Forecasting ozone concentrations is crucial for issuing timely warnings and advisories, enabling vulnerable populations to avoid outdoor activities during periods of high ozone (Vicente et al., 2024).

In light of the growing concern over air pollution, numerous studies have been undertaken to better understand and mitigate its impacts. A notable contribution to this field comes from the research of Hadian and Moradizadeh (2023), who conducted a study modeling the spatial distribution of nitrogen dioxide (NO_2) and ozone (O_3) pollutants. They achieved this by combining data from ground-based monitoring stations and high-resolution Sentinel-5 satellites. The Kriging interpolation method was employed to estimate pollutant concentrations between monitoring stations. The model demonstrated a robust performance, with Root Mean Square Errors (RMSE) of 2.79 ppb for NO_2 and 0.86 ppb for O_3, indicating a strong correlation between the predicted and observed values. Ghanbari and Eisazadeh (2021) focused on modeling the concentration density of ozone and nitrogen oxide using Geographic Information Systems (GIS) and compared their results with Sentinel-5 data on Google Earth Engine. They utilized two methods: Inverse Distance Weighting (IDW) and Sentinel-5P NRTI O_3: Near Real Time. The model exhibited the best performance in 2008

(R^2=0.9188) and 2009 (R^2=0.9134), while the worst performance was observed in 2018 (R^2=0.476), suggesting potential variations in model accuracy over time. Gharibi and Shayesteh (2021) focused on using Sentinel-5 satellite images to identify air pollution hotspots in Iran. To assess clustering patterns, the G statistic was used, and Gi statistics were employed to identify hot spots for each pollutant within a GIS environment. The spatial distribution pattern of pollutants was determined using the Moran's I index. The results of the G statistic showed that the pollutants exhibited a clustered distribution pattern and spatial autocorrelation (Moran's I=0.72). Rais-Pour and Asakereh (2020) investigated the satellite-based monitoring of ozone layer changes in Iran's atmosphere. Data from the AIRS instrument on the AQUA satellite was used to analyze ozone trends over Iran. The findings indicated a yearly decline in ozone levels in Iran's atmosphere. Spatially, ozone levels generally increased from south to north. Wang et al (2022) developed a machine-learning model to estimate ground-level ozone concentrations in California using TROPOMI and high-resolution meteorological data. By utilizing the total ozone column from TROPOMI along with ozone profile information retrieved by the Ozone Monitoring Instrument (OMI), they created a model to predict daily maximum 8-hour average ground-level ozone concentrations with a 10 km spatial resolution. The model's validation resulted in an R^2 of 0.84 and an RMSE of 0.0059 ppb, indicating a good agreement between model predictions and observations. Quesada-Ruiz et al (2019) examined the benefits of ozone observations from Sentinel-5 and future Sentinel-4 missions in the troposphere. Simulated data consisting of six eigenvectors were used to minimize the dataset size by removing the noise-dominated part of the observations. The results demonstrated that satellite data clearly provide a direct added value at around 200 hPa for the entire absorption period and the entire European domain. Zhao et al. (2021) investigated tropospheric ozone changes during the COVID-19 pandemic in China. This paper presents tropospheric ozone profiles and columns retrieved from UV radiation measured by the TROPOMI instrument on the Sentinel-5 satellite based on the optimal estimation method. The results showed that both the tropospheric ozone column and stratospheric ozone have a very good agreement with the validation data and also tropospheric ozone as the primary option of secondary air pollutants did not decrease simultaneously but increased in some areas.

Among various methods for monitoring air pollution, remote sensing techniques using instruments and technologies have gained significant importance due to the continuous nature of their data generation in both time and space. In these methods, information about air pollutants is transmitted through electromagnetic radiation, allowing for high spatial and temporal resolution data collection, as well as vertical profile measurements (Saxena and Naik, 2019). Satellite-based remote sensing of air pollutants and trace gases provides a suitable platform for understanding the current state of air quality and future climate change on a global scale. On the other hand, achieving the highest possible accuracy in pollutant monitoring is crucial due to various considerations such as chemical composition, lifetime, emission sources, and so on (Saxena and Naik, 2019). In this study, the GEE system was used to prepare all information data. GEE is an open-source spatial analysis platform that enables users to visualize and analyze satellite images of the planet earth. The many capabilities of the Google Earth Engine system have been reviewed and approved for checking all kinds of hydrometeorology and hydrological criteria (Yousefi et al., 2022).

The examination of these issues and challenges using the most advanced online geographic information systems (SOGIS) has significantly accelerated the problem-solving process. In contrast, in the past, these problems were analyzed and solved slowly and over a long period using desktop software (Jamali and Abdolkhani, 2009). Remote sensing methods utilize satellite data and images to monitor various quantities, including pollution monitoring. Satellite data, due to their free availability, high spatial resolution, and wide coverage of the study area, can be used for medium-term and long-term forecasting and early warning regarding air quality (Xian, 2015). On the other hand, satellites, by orbiting the Earth and monitoring the same area at different times, provide the opportunity to conduct studies over various periods. Long-term studies of pollutants are important in providing accurate information to managers in

order to develop strategies to control air pollution crises. One of the newest satellites for air pollution monitoring is Sentinel-5, part of the European Space Agency's Copernicus program. Since its launch in 2018, Sentinel-5 has provided reliable and efficient data for studying atmospheric aerosols, Sulfur dioxide, nitrogen dioxide, carbon monoxide, and ozone. Therefore, by processing data from this satellite, valuable information about air pollutants can be obtained (Theys et al., 2016). In this research, the objective is to evaluate the capabilities of the TROPOMI sensor on Sentinel-5 for air pollution monitoring and to examine trends in pollutant levels in the study area. The results of this research can provide a suitable tool for offering solutions to policymakers at various levels.

2. Material and Methods

In this research, Level 3 (L3) images from the TROPOMI (Tropospheric Monitoring Instrument) sensor the Sentinel-5 satellite were used to monitor pollutant concentrations (https:// developer s.google.com /earth-engine /datasets/ catalog). All S5P datasets, except for CH_4, have two versions: Near Real-Time (NRTI) and Offline (OFFL). Only CH_4 data is available in the OFFL version. NRTI data covers a smaller area compared to OFFL data but becomes available faster after acquisition. OFFL data contains data from one orbit (which, due to half the Earth being dark, only contains data from one hemisphere).

The bands used in this study to extract different pollutants are presented in Table 1.

This study initially used the Python programming language within the Google Earth Engine (GEE) platform to retrieve satellite images of CO, SO_2, NO_2, and O_3 pollutant concentrations. Various products, as listed in Table 1, were called within the study region's boundaries over the specified period to monitor atmospheric pollutants and identify pollution sources in the province. Consequently, a raw function was defined for each Sentinel-5 product. In each function, the average pollutant concentration was calculated within the study boundaries and the defined time frame. Each function had multiple inputs, with the first input being a dataset that included satellite images with a start time (10/07/2018) and an end time (30/12/2023). Each function was also applied to a specific band associated with the pollutant image set in question. Therefore, for each pollutant, there was a specific dataset and band based on Table 1. Another variable was defined to clip the retrieved satellite images, resulting from the first variable, based on the study boundaries. The output variable was also a set of retrieved images defined within the specified temporal and spatial filter with a spatial resolution of one kilometer. The output obtained from the average pollutant concentration for the period from 10/07/2018 to 30/12/2023 was calculated in these filters. Then, the spatial map of the average pollutant concentration was analyzed in ArcMap software.

Table 1. Specifications of Sentinel-5 satellite products for CO, NO_2, SO_2 and O_3 pollutants

Product	Data set	Bond	Unit	Min	Max	Description
Sentinel-5P NRTI CO: Near Real-Time Carbon Monoxide	COPERNICUS /S5P/NRTI/L3 _CO	CO_column_number_density	mol/m^2	-279	4.64	Vertically integrated CO column density.
Sentinel-5P NRTI NO_2: Near Real-Time Nitrogen Dioxide	COPERNICUS /S5P/NRTI/L3 _ NO_2	NO_2_column_number_density	mol/m^2	-0.0006	0.0096	Total vertical column of NO_2 (ratio of the slant column density of NO2 and the total air mass factor)
Sentinel-5P NRTI SO_2: Near Real-Time Sulphur Dioxide	COPERNICUS /S5P/NRTI/L3 _ SO_2	SO_2_column_number_density	mol/m^2	-48	0.24	Total atmospheric column of O_3 between the surface and the top of the atmosphere, calculated with the DOAS algorithm vertical column density, calculated using the DOAS technique.
Sentinel-5P NRTI O_3: Near Real-Time Ozone	COPERNICUS /S5P/NRTI/L3 _O_3	O_3_column_number_density	mol/m^2	0.0047	0.272	

This study initially used the Python programming language within the Google Earth Engine (GEE) platform to retrieve satellite images of CO, SO_2, NO_2, and O_3 pollutant concentrations. Various products, as listed in Table 1, were called within the study region's boundaries over the specified period to monitor atmospheric pollutants and identify pollution sources in the province. Consequently, a raw function was defined for each Sentinel-5 product. In each function, the average pollutant concentration was calculated within the study boundaries and the defined time frame. Each function had multiple inputs, with the first input being a dataset that included satellite images with a start time (10/07/2018) and an end time (30/12/2023). Each function was also applied to a specific band associated with the pollutant image set in question. Therefore, for each pollutant, there was a specific dataset and band based on Table 1. Another variable was defined to clip the retrieved satellite images, resulting from the first variable, based on the study boundaries. The output variable was also a set of retrieved images defined within the specified temporal and spatial filter with a spatial resolution of one kilometer. The output obtained from the average pollutant concentration for the period from 10/07/2018 to 30/12/2023 was calculated in these filters. Then, the spatial map of the average pollutant concentration was analyzed in ArcMap software.

2.1. GIS technology and spatial modeling

GIS provides spatial information, patterns, and sensitivity to incident variables. These are essential for future initiatives and planning to reduce spatial vulnerability and promote sustainable development. GIS technology also provides for management strategies and executive tasks that are vital in the field of disaster management. In addition, spatio-temporal mapping of disaster variables may provide historical trends in hazard severity, magnitude, and area.

2.2. Inverse distance weighted model (IDW)

A deterministic interpolation model is used to evaluate the spatial sensitivity, pattern, variability, and concentration of georeferenced variables. This model is used to quantify the weighted values of the unsampled points through the inverse distance function of the values of the spatial graticule reference points (Gong G et al., 2014). Equation (1) is calculated for the weight power (ki) of the IDW model.

$$\lambda_{\mathrm{i}} = (\mathrm{D_i} - \alpha)\lambda_{\mathrm{i}} = (\mathrm{D_i} - \alpha)/\sum_{i=1}^{\mathrm{n}} \mathrm{D_i} - \alpha \qquad (1)$$

In equation (1), λi is the weight of station i, Di is the distance from the station to the unknown point, and α is the weighting power.

2.3. Validation

To validate the results obtained in this study, five ground-based air quality monitoring stations in Razavi and South Khorasan Provinces were selected. The accuracy of the monitoring results from these five stations was compared with satellite-based monitoring using Sentinel-5's TROPOMI imagery. The coefficient of determination (R^2) was calculated using equation (2) to assess the level of agreement between the two datasets.

$$R^r = \left(\frac{\sum_{i=1}^{n} (Xi - \overline{X_1})(Yi - \bar{Y}i)}{\sqrt{\sum_{i=1}^{n} (Xi - \bar{X}i)^r \cdot \sqrt{\sum_{i=1}^{n} (Yi - \bar{Y}i)}^r}} \right)^r \qquad (2)$$

n represents the number of data, $\overline{X}$i is the average pollutant of the station, $\overline{Y}$i is the average pollutant calculated from the meter Xi is the pollutant values of the station and Yi is the pollutant values calculated from the meter.

2.3. Study area

Fig. 1 show the location of the studied area of Razavi and South Khorasan provinces; The area of South Khorasan province is 151.913 km^2 and Razavi Khorasan is 117.769 km^2. South Khorasan province is located in the east of Iran and on the northeastern edge of the Lot plain. The location of South Khorasan province is limited to Razavi Khorasan province from the north, Afghanistan province from the east, Kerman and Sistan and Baluchistan provinces from the south, and Yazd and Isfahan provinces from the west. The location of Razavi Khorasan province is limited to North Khorasan province and Turkmenistan country from the north, Afghanistan and Turkmenistan countries from the east, South Khorasan province from the south, and Semnan province from the west. In terms of geographical location, South Khorasan

province is between 31°20' to 33°31' north latitude and 57°57' to 59°40' east longitude, and Razavi Khorasan province is between 56°19' to 61°16' east longitude and 33°52' minutes to 37°42' north latitude.

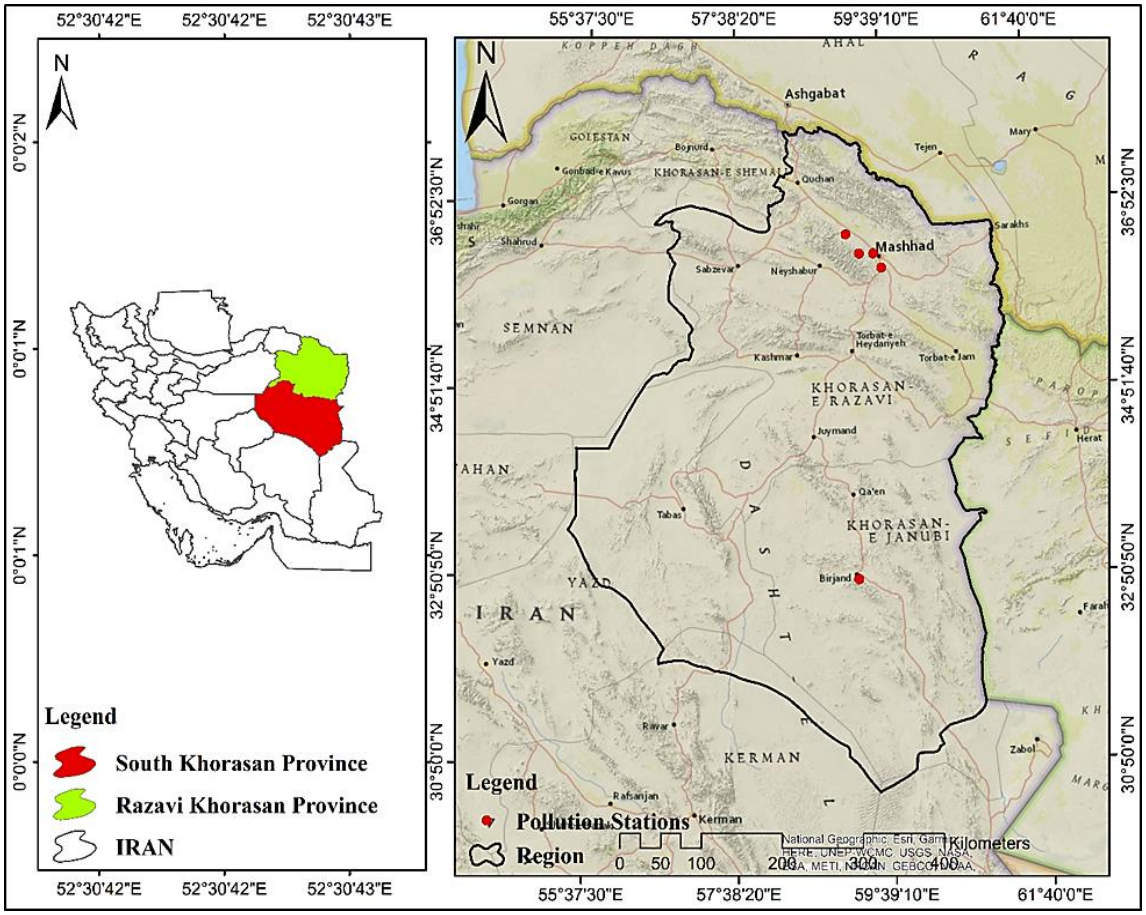

Fig. 1. Location of the study area

3. Results and discussion

After executing the programming in the GEE environment, spatial maps of pollutant hotspots for CO, NO_2, O_3, and SO_2 were produced separately based on the average concentration of each pollutant from 2018 to 2023. Subsequently, to identify the hotspots of all pollutants, raster maps for each pollutant were created in Fig. 2.

The GEE platform provides high-resolution images of CO concentrations. Carbon monoxide (CO) is an important atmospheric trace gas for understanding tropospheric chemistry. In some urban areas, it is the main air pollutant. TROPOMI on the Sentinel 5 Precursor (S5P) satellite observes global CO abundance by exploiting ground-based radiance measurements in the shortwave infrared (SWIR) 2.3-micrometer spectral range of the solar spectrum in both clear and cloudy skies. TROPOMI clear-sky observations provide total CO columns with sensitivity to the tropospheric boundary layer. For cloudy atmospheres, column sensitivity varies with the light path. Fig. 2a show a spatial map of carbon monoxide, where the highest levels of this pollutant are observed in the north, northwest, center (Khorasan Razavi province), and northwest and west of South Khorasan province. The amount of CO pollutant has increased from Khorasan Razavi province to South Khorasan province. This dataset provides real-time high-resolution images of the total ozone column. In the stratosphere, the ozone layer protects the biosphere from harmful ultraviolet solar radiation. In the troposphere, it acts as an efficient cleansing agent, but at high concentrations, it is also harmful to human

health, animals, and vegetation. Ozone is also a significant greenhouse gas contributing to climate change. Since the discovery of the Antarctic ozone hole in the 1980s and the subsequent Montreal Protocol, which regulates the production of ozone-depleting substances containing chlorine, ozone has been routinely monitored from the ground and from space. Fig. 2b shows a spatial map of ozone. An examination of ozone pollution hotspots indicates that the amount of this pollutant has increased from South Khorasan Province to Khorasan Razavi Province, with the highest amount of ozone recorded in the north and northeast of Khorasan Razavi Province.

This dataset provides near real-time, high-resolution images of NO_2 concentrations. Nitrogen oxides (NO_2 and NO) are crucial trace gases in the Earth's atmosphere, present in both the troposphere and stratosphere. These gases enter the atmosphere as a result of human activities (primarily the combustion of fossil fuels and biomass burning) and natural processes (wildfires, lightning, and microbiological processes in the soil). NO_2 is used to represent the concentration of total nitrogen oxides because, during the day in the presence of sunlight, a photochemical cycle involving ozone (O_3) converts NO to NO_2 and vice versa on a timescale of several minutes.

Fig. 2c shows the spatial map of nitrogen dioxide. The highest levels of NO_2 pollutants were recorded in the northwest and central regions of Khorasan Razavi province, and the amount of this pollutant decreases from Khorasan Razavi province to South Khorasan province. This dataset provides near real-time high-resolution images of atmospheric sulfur dioxide (SO_2) concentrations. Sulfur dioxide (SO_2) enters the Earth's atmosphere through natural and human processes. SO_2 plays an important role in local and global scale chemistry and its effects range from short-term pollution to impacts on climate. Only about 30% of the SO_2 emitted comes from natural sources, and the majority is of human origin. SO_2 emissions negatively affect human health and air quality. SO_2 affects the climate through radiative forcing and the formation of sulfate aerosols. SO_2 emissions, along with volcanic ash, can also pose a threat to aviation activities. The S5P/TROPOMI satellite samples the Earth's surface with a revisit time of one day and a spatial resolution of 3.5x7 km, which allows for detailed feature discrimination, including the detection of much smaller SO_2 columns. Fig. 2d shows a spatial map of sulfur dioxide. According to the results, the highest amount of this pollutant was recorded in the city of Mashhad, Khorasan Razavi province.

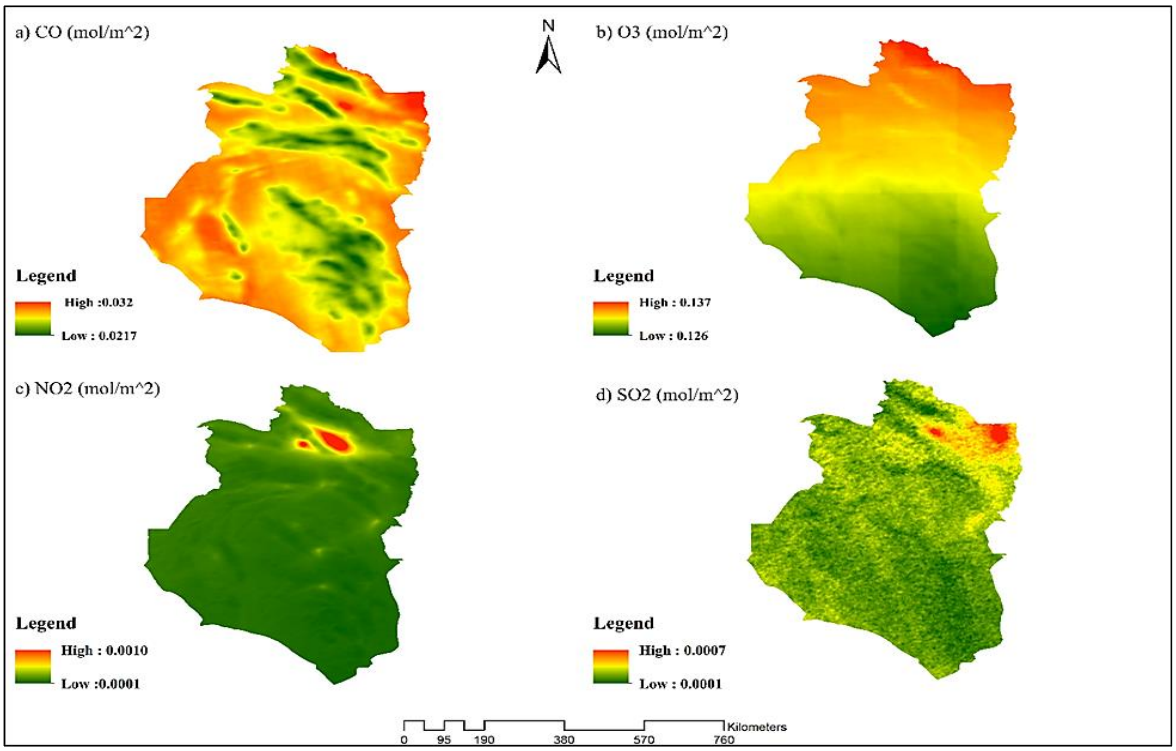

Fig. 2. Hotspots of CO, NO_2, O_3, and SO_2 pollutants in the Razavi and South Khorasan Provinces

3.1. Regional Analysis of County Contributions to Air Pollutants

Fig. 3 shows maps of the average concentration of each pollutant based on the Border working units of provinces and cities from 2018 to 2023. The value of each pixel in each region represents the average concentration of pollutants in that area. The highest share of nitrogen dioxide comes from the counties of Mashhad, Binalood, Golbahar, and Nishapur in Khorasan Razavi province. The highest share of carbon monoxide comes from the counties of Sarakhs, Kalat, Dargaz, Mashhad, and Binalood in Khorasan Razavi province and the county of Tabas in South Khorasan province. The highest share of sulfur dioxide comes from the county of Sarakhs in Khorasan Razavi province. Also, the highest share of the ozone pollutants comes from the counties of Sarakhs, Kalat, Dargaz, and Quchan in Khorasan Razavi province.

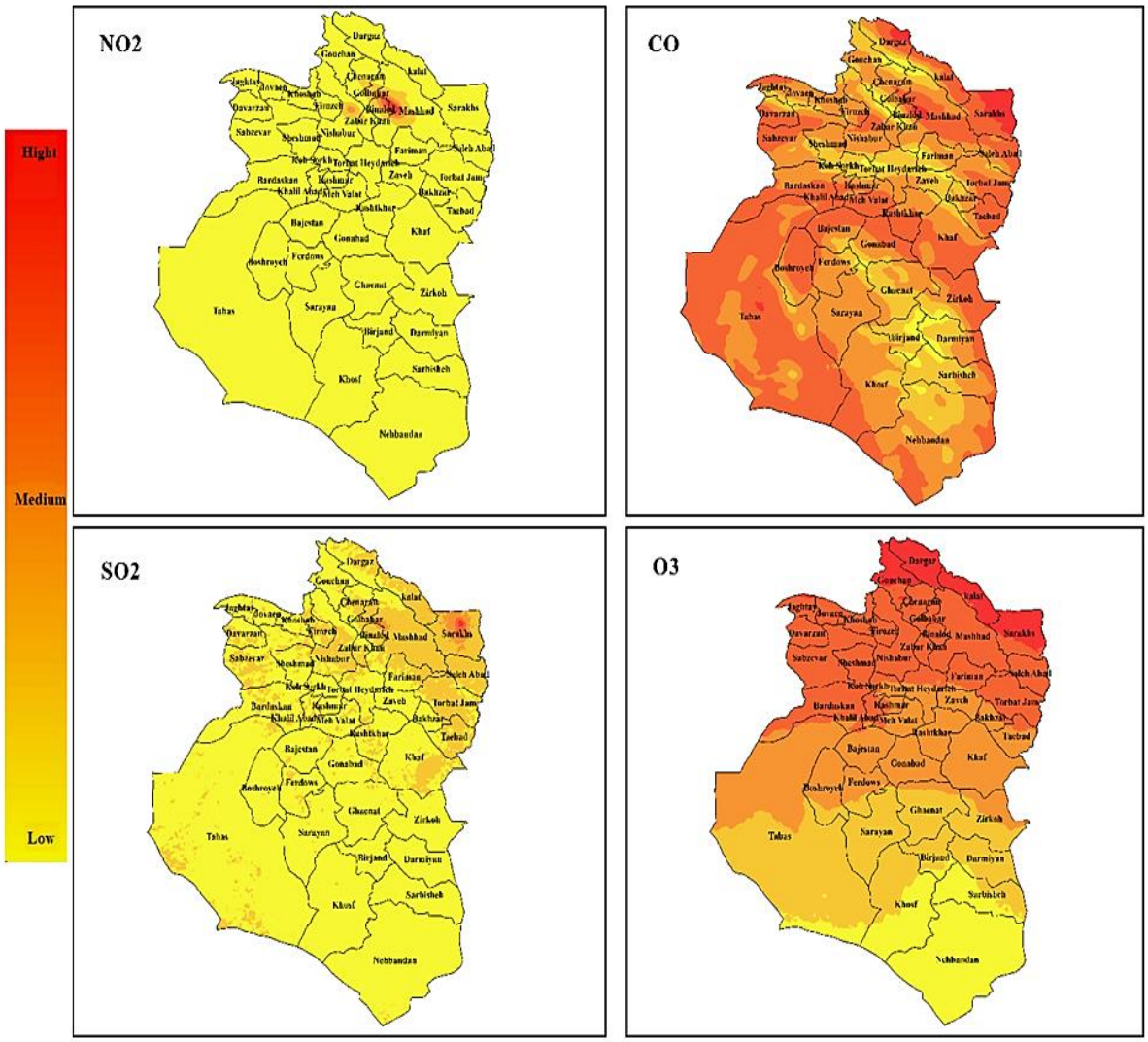

Fig. 3. Contribution of air pollutants based on county boundaries in Razavi and South Khorasan Provinces

3.2. Slope of Annual Average Pollutant Changes

The results of air pollutant monitoring using Sentinel-5 images between 2018 and 2023 are shown in Fig. 4, Fig. 5, Fig. 6, and Fig.7 In these diagrams, the daily concentration values of pollutants are displayed annually. The range of annual average changes in CO pollutant levels from 2018 to 2023 is between 0.024 and 0.032 mol/m², O_3 pollutants between 0.118 and 0.152 mol/m², NO_2 pollutants between 0.0001 and 0.0010 mol/m², and SO_2 pollutant between 0.001 and 0.007 mol/m².

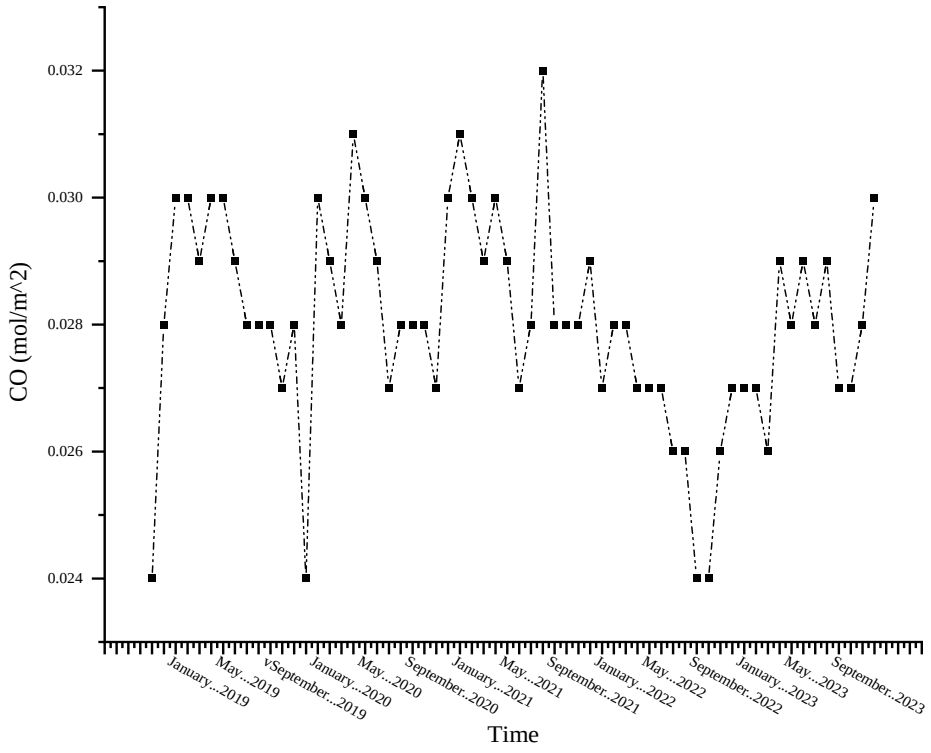

Fig. 4. Annual average changes in atmospheric CO pollutants between 2018 and 2023

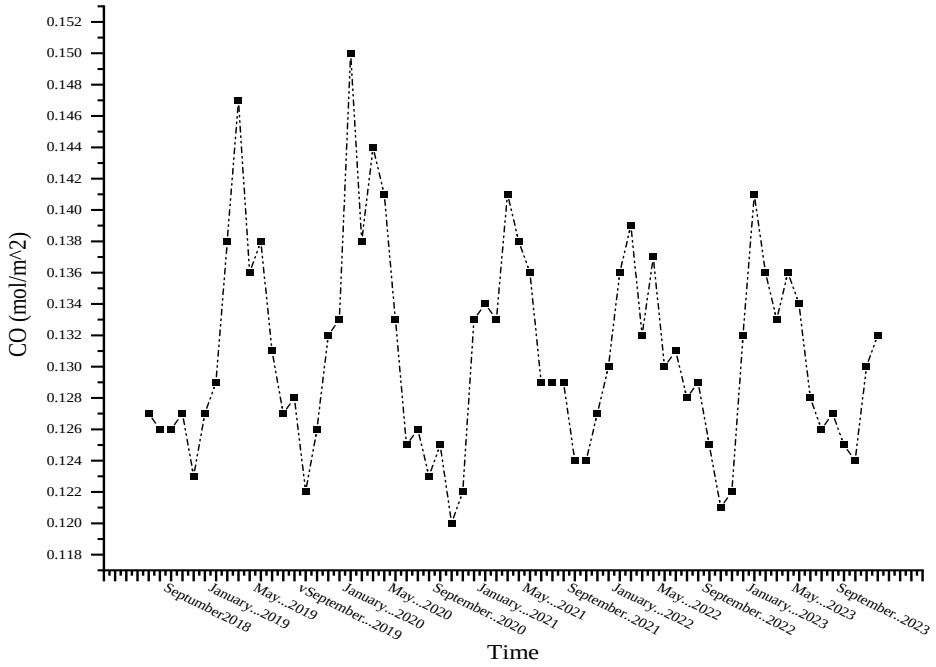

Fig. 5. Annual average changes in atmospheric O_3 pollutants between 2018 and 2023

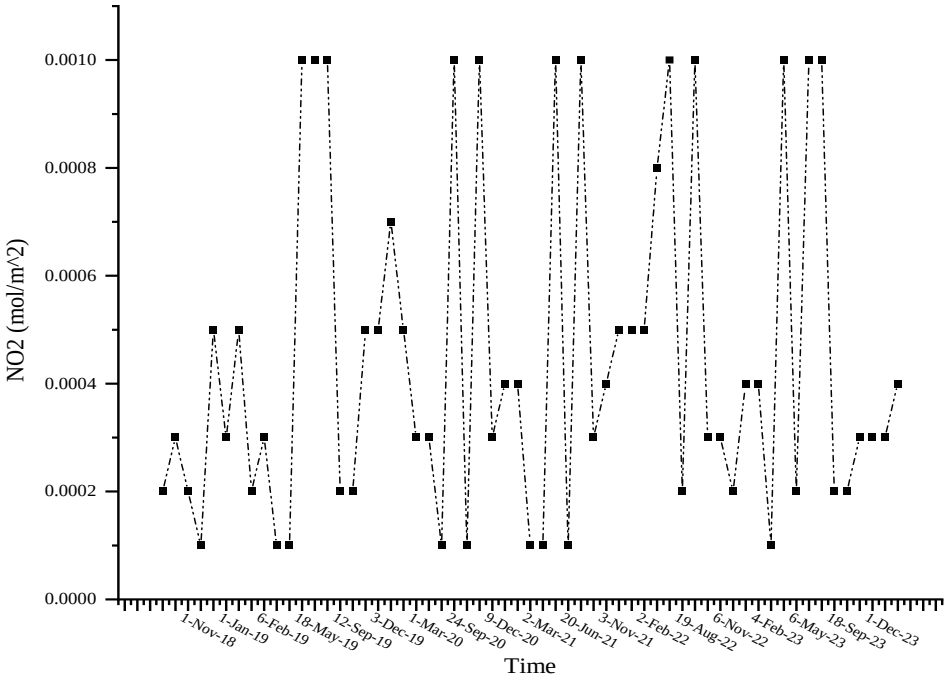

Fig. 6. Annual average changes in atmospheric NO_2 pollutants between 2018 and 2023

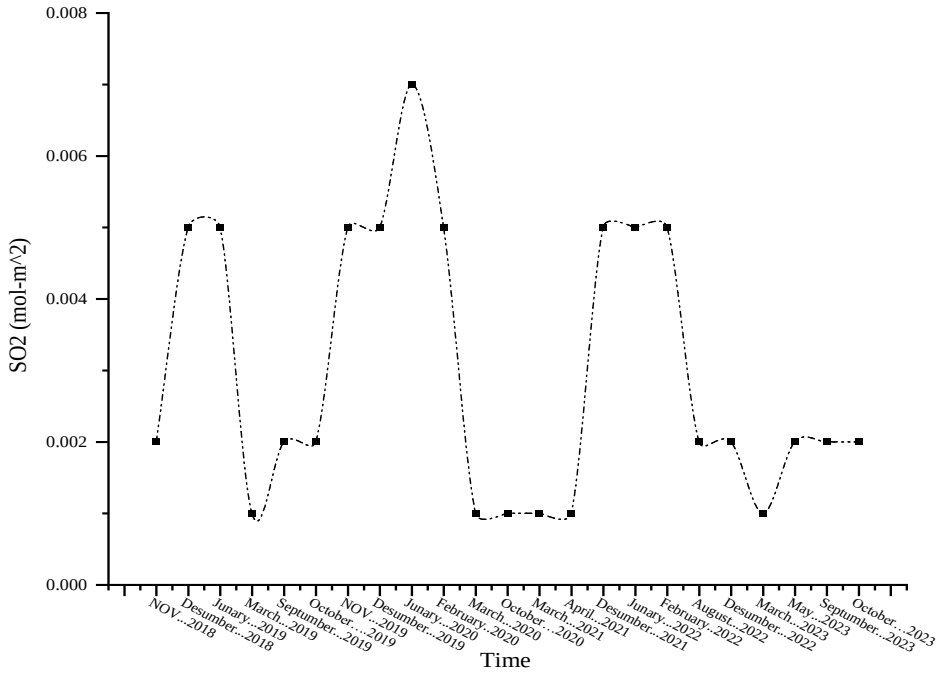

Fig. 7. Annual average changes in atmospheric SO_2 pollutants between 2018 and 2023

3.3. Heatmap

The term "heatmap" has been used in statistical analyses for many years. It is a statistical matrix used to show the correlation between different variables (Dziuda, 2010). This visualization method is defined as "a graphical display of data where values in a matrix are represented as colors". Wilkinson and Friendly (2009) find "the earliest sources of this display in late 19th century publications" and calls them "the most widely used displays in bioinformatics". Ultimately, this form of statistical analysis evolved into the creation of cartographic heat maps. Heatmaps are so named because of their color schemes, which change from blue to red with increasing values, giving a "warmer" appearance (DeBoer, 2015). Heatmaps have become one of the most popular methods for data representation. A heatmap is a graphical representation of data where values contained in a matrix are represented as colors. Numerous variations of heatmaps exist, such as web heatmaps and treemaps (Zhao et al., 2014), which provide a more visually appealing representation for spatiotemporal analysis. conventional charts, such as scatter plots and line charts, are commonly used for exploratory analysis of air pollution time series data without spatial analysis (Janssen et al., 2013). However, after analyzing the characteristics of different chart types, researchers have found that heatmaps are very suitable for displaying time series data and that a calendar view is useful for displaying years of daily data (Van Wijk and Van Selow, 1999). This method presents a novel perspective on time series data and a tool for comprehensively understanding ordinary line charts or matrix charts that are not presented due to the fact that the data is divided into several sections based on season or year. Fig. 8 shows the analysis of heat maps on each of the pollutants in the period considered. Red (hot) spots have larger values, and this period has a higher pollution status compared to other times. Blue (cold) spots have smaller values, and the pollution status is lower compared to other times. As can be seen, the amount of air pollutants (CO, O_3, NO_2, and SO_2) has increased from 2018 to 2023.

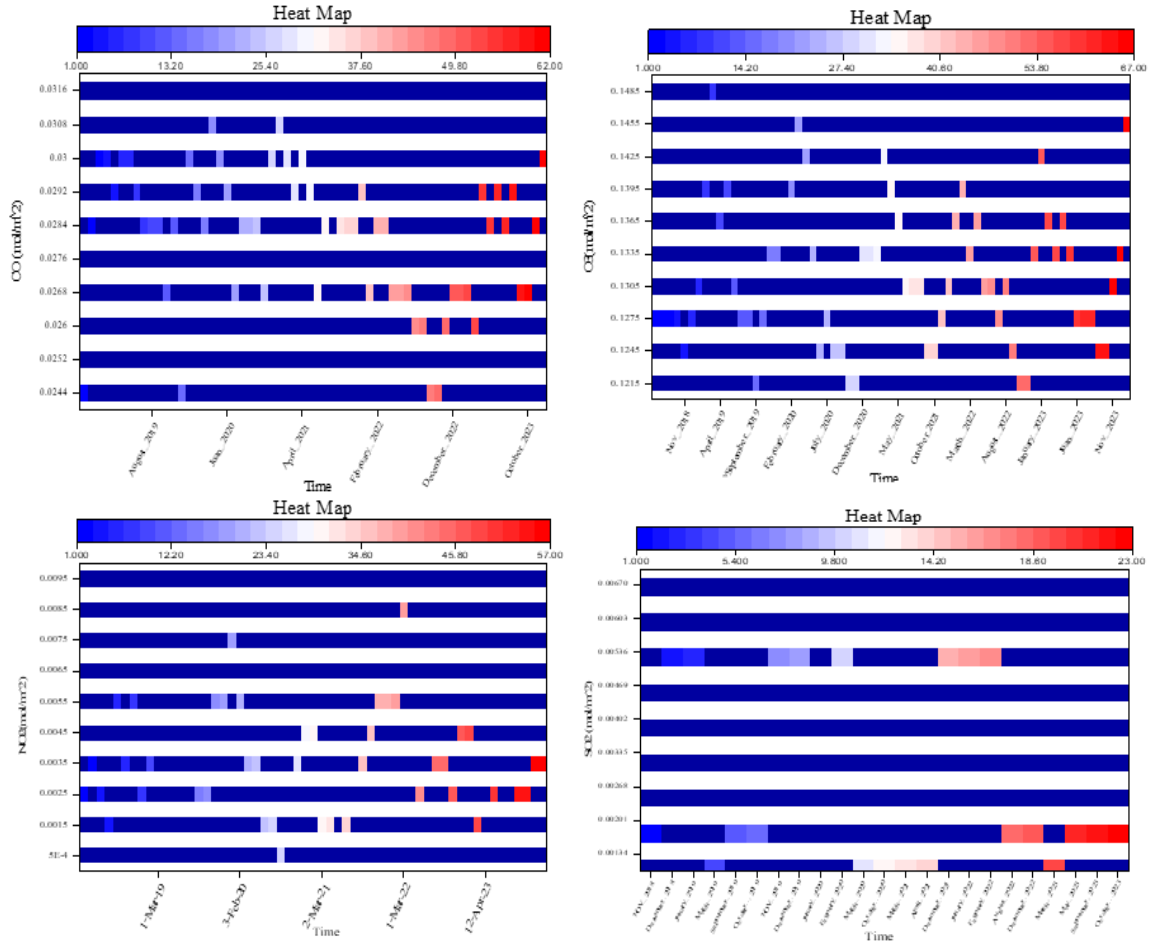

Fig. 8. Cluster analysis of heatmaps for CO, O_3, NO_2, and SO_2 pollutants based on year and mont

To further analyze and analyze the results obtained in this research using Sentinel-5 TROPOMI sensor images, five terrestrial air pollution monitoring stations were selected in Razavi and South Khorasan Provinces, and the monitoring results of these five stations were compared with satellite. Pollutant-based monitoring using Sentinel-5 imagery. The spatial distribution of the measured concentrations of pollutants (CO, O_3, NO_2, and SO_2) for the period 2018 to 2023 is shown in Fig. 9 According to the results obtained based on Fig. 9a, it can be said that the red areas are large urban areas and the amount of CO pollution in these areas is higher than other areas. Therefore, the Sajjad and Khayyam stations have more CO_2 pollution than the other two stations. Toruq and machine tool stations have average concentration and dispersion of this pollutant, and the amount of CO in these two stations is close, while Birjand station has the lowest amount of this pollutant in the studied area. Also, according to the study of Kafi et al. (2023) in connection with the thermal map of a part of the studied area and comparing its results with the final ozone map, it is clear that areas with higher temperatures have higher ozone levels.

Furthermore, based on Fig. 9b, we can conclude that the machine tool station contains the highest amount of O_3 pollutants compared to the other four stations. The Toruq station has a moderate concentration and distribution of this pollutant, and the amount of this pollutant in the Birjand station is lower than other stations. Similarly, in Fig. 9c, it is observed that the machine tool and Toruq stations have the highest amount of NO_2 pollutants. The Khayyam, Sajjad, and Birjand stations have a moderate concentration and distribution of this pollutant, and the amount of NO_2 in these three air quality monitoring stations is similar. Based on Fig. 9d, it can be stated that the Toruq station contains the highest amount of SO_2 pollutants. Also, the Khayyam and Sejad stations are in a moderate state in terms of the concentration and distribution of this pollutant. Similarly, the Machine Tools and Birjand stations are stations with the lowest levels of SO_2 pollutants. In this study, the role of satellite remote sensing in air quality monitoring is evident. Table 2 shows that the results obtained from Sentinel-5 satellite images have sufficient reliability, and therefore, this tool can be used in continuous monitoring and management of air quality in the country. With the development of powerful cloud processing systems such as the Google Earth Engine platform, free services of this system can be used in heavy processing. On the other hand, considering the low density and sometimes the inappropriate distribution of ground-based air quality monitoring stations, the use of free Sentinel-5 images in monitoring changes in pollutant concentrations in all parts of the country can be beneficial. Also, a comparison of the results of the TROPOMI sensor (Fig. 2) and the IDW model (ground data, Fig. 9) confirms the accuracy of the monitoring performed using Sentinel-5 satellite images.

Table 2. Results of the coefficient of determination (R^2) between ground observations and Sentinel-5 satellite images

SO_2	**NO_2**	**O_3**	**CO**	**The Pollutant**
0.78	0.79	0.85	0.76	Coefficient of determination (R2)

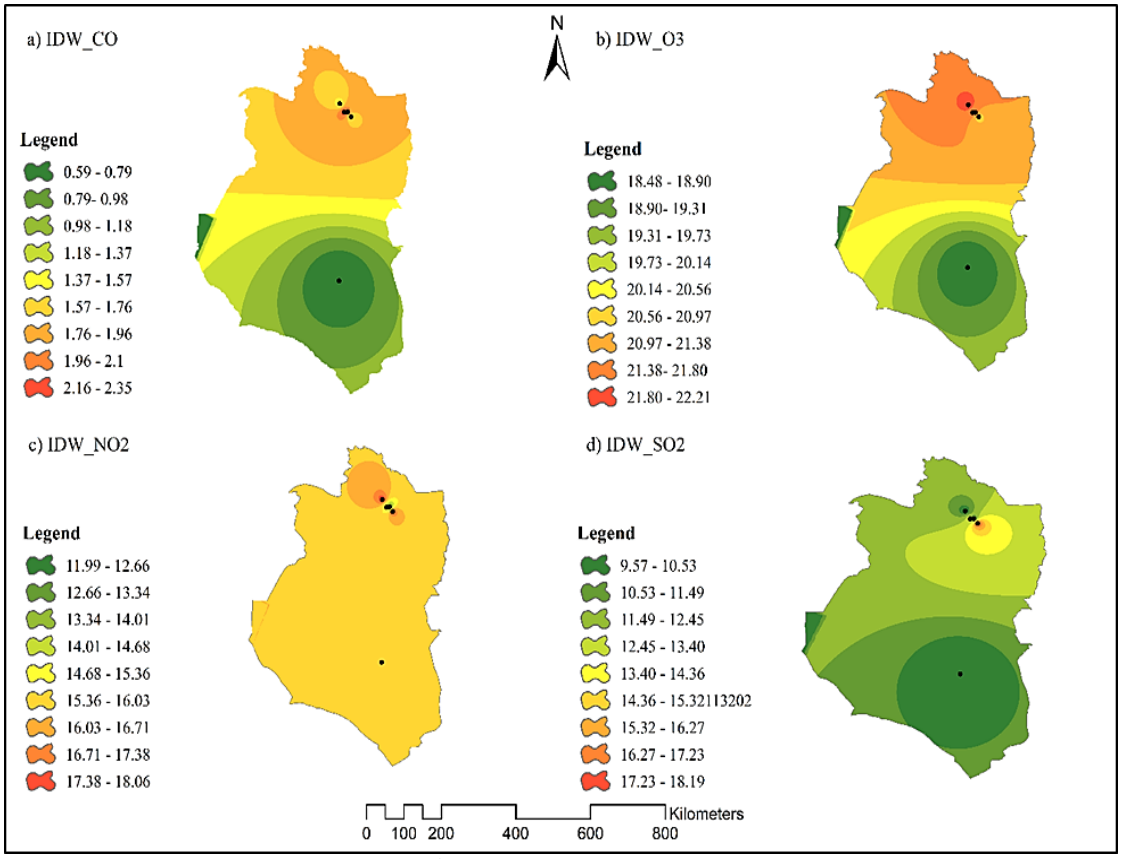

Fig. 9. Spatial distribution of measured pollutant concentrations using the IDW model

4. Conclusion

Air quality monitoring stations measure pollutant concentrations at specific points, thus providing high accuracy. However, they only cover the areas around the stations and are unable to estimate pollutant levels at distances farther from the stations. Therefore, relying solely on the measurements of these stations cannot identify pollution sources. The results of pollutant dispersion in the study area indicate that estimating the average pollutant concentration using remote sensing images can be very important for identifying pollution sources. Therefore, it is necessary to use continuous images that measure pollutant levels in the atmosphere daily to locate atmospheric pollutant sources. Accurate measurement of air pollutants with high spatial and temporal resolution to determine how Their distribution and effectiveness, as well as provide solutions for managers at the provincial and national levels, are essential. The use of tools and technologies based on remote sensing is of great importance due to the nature of continuous temporal and spatial data production. Sentinel-5 satellite has a high capability in imaging and monitoring a large number of rare gases as well as suspended particles. Therefore, satellite images for monitoring air pollutants and locations can be very fruitful at a low cost and time-consuming. In this research, the capability of the TROPOMI sensor on Sentinel-5 satellite in monitoring air pollution (four pollutants: CO, O_3, NO_2, and SO_2) from 2018 to 2023 has been evaluated. Moreover, the trend of changes in some pollutants in the Razavi and South Khorasan Provinces over the past five years has been investigated. The monitoring shows that Mashhad is the most polluted city in the study area from 2018 to 2023. Furthermore, regional analysis of the share of counties in air pollutants revealed that the highest share of nitrogen dioxide belongs to the counties of Mashhad, Binālod, Golbahar, and Nīshābūr in Razavi Khorasan Province. The highest share of carbon monoxide belongs to the counties of Sarakhs, Kalāt, Dargaz, Mashhad, and Binālod in Razavi Khorasan Province, and the county of Tabas in South Khorasan Province. The highest contribution of sulfur dioxide was observed in Sarkhes County, Khorasan Razavi Province. The highest contribution of ozone was observed

in Sarkhes, Kalat, Dargaz, and Quchan counties of Khorasan Razavi Province. The spatial distribution of pollutant concentrations showed an increase from South Khorasan Province to Razavi Khorasan Province, with the highest values recorded in the north, northeast, and center of Khorasan Razavi Province which is confirmed according to Gharibi and Shayesteh (2022) studies. Additionally, the spatial distribution of pollutant concentrations measured using the IDW model indicated the highest concentrations at the Mashin-e-Abzar, Khiam, Sajjad, and Tarq monitoring stations. Furthermore, based on the extracted heat maps, the level of pollutants has increased from 2018 to 2023. The main source of this increase can be attributed to the population, industrial expansion, and the general increase in human and industrial activities, which is confirmed according to the studies of Shami et al (2021). To evaluate the accuracy of the monitoring conducted using Sentinel-5 satellite images, five air quality monitoring stations in Razavi and South Khorasan Provinces were used. The results showed that the measurements obtained using Sentinel-5 images had a correlation of at least 0.76% for CO, 0.85% for O_3, 0.79% for NO_2, and 0.78% for SO_2 compared to the measurements made by the air quality monitoring stations.

Acknowledgments

This research is not under any financial support. We thank the University of Birjand for its spiritual support in conducting this research.

References

Aljanabi, M., Shkoukani, M. & Hijjawi, M., 2020. Ground-level Ozone Prediction Using Machine Learning Techniques: A Case Study in Amman, Jordan. *International Journal of Automation and Computing*, 17, 667-677.

Carbo-Bustinza, N., Belmonte, M., Jimenez, V., Montalban, P., Rivera, M., Martínez, F. G., Mohamed, M.M.H., De La Cruz, A.R.H., da Costa, K. & López-Gonzales, J.L., 2022. A machine learning approach to analyse ozone concentration in metropolitan area of Lima, Peru. *Scientific Reports*, 12.

Cheng, M., Fang, F., Navon, I. M., Zheng, J., Zhu, J. & Pain, C., 2023. Assessing uncertainty and heterogeneity in machine learning-based spatiotemporal ozone prediction in Beijing-Tianjin-Hebei region in China. *Science of the Total Environment*, 881, 163146.

DeBoer, M., 2015. Understanding the Heat Map. *Cartographic Perspectives*, 39-43.

Dickerson, R.R., Anderson, D.C. & Ren, X., 2019. On the use of data from commercial NOx analyzers for air pollution studies. *Atmospheric Environment*, 214, 116873.

Dziuda, D.M., 2010. Data mining for genomics and proteomics: analysis of gene and protein expression data. John Wiley & Sons.

Ehteram, M., Najah Ahmed, A., Sheikh Khozani, Z. & El-Shafie, A., 2023. Graph convolutional network – Long Short-Term Memory Neural Network- Multi Layer Perceptron Gaussian progress regression model: A new deep learning model for predicting ozone concertation.

Ezimand, K., Kakroodi, A., 2019. Prediction and spatio–temporal analysis of ozone concentration in a metropolitan area. *Ecological Indicators*, 103, 589–598.

Finney, D.L., Doherty, R.M., Wild, O., Young, P.J. & Butler, A., 2016. Response of lightning NOx emissions and ozone production to climate change: Insights from the Atmospheric Chemistry and Climate Model Intercomparison Project. *Geophysical Research Letters*, 43, 5492-5500.

Ghanbari, A. & Esazadeh, V., 2021. Modeling the concentration of ozone and nitrogen oxide pollutants in GIS and comparing these pollutant concentrations with the Sentinel-5 product in the Google Earth Engine system - the study area: Tehran. Scientific-Research Quarterly of Geographical Information "Sephehr", 30, 247-261.

Gharibi, Sh. & Shayesteh, K., 2021. The application of Sentinel-5 satellite images in identifying air pollution hotspots in Iran. *Spatial Analysis of Environmental Hazards*, 31, 123-138.

Gong, G., Mattevada, S. & O'Bryant, S.E., 2014. Comparison of the accuracy of kriging and IDW interpolations in estimating groundwater arsenic concentrations in Texas. Environmental research, 130, 59-69.

Greenberg, N., Carel, R.S., Derazne, E., Bibi, H., Shpriz, M., Tzur, D. & Portnov, B.A., 2016. Different effects of long-term exposures to SO_2 and NO_2 air pollutants on asthma severity in young adults. Journal of toxicology and environmental health, Part A, 79, 342-351.

Grewe, V., Dahlmann, K., Matthes, S. & Steinbrecht, W., 2012. Attributing ozone to NOx emissions: Implications for climate mitigation measures. Atmospheric Environment, 59, 102-107.

Hadian, A. & Moradizadeh, M., 2024. Modeling the concentration distribution of NO_2 and O_3 pollutants with appropriate spatial resolution using ground and satellite data integration. *Iranian Journal of Remote Sensing & GIS*, 16(2), 85-104.

Jamali, A. & Abdolkhani, A., 2009. Preparedness against landslide disasters with mapping of landslide potential by GIS-SMCE (Yazd-Iran). *International Journal of Geoinformatics*, 5, 25-31.

Janssen, N.A., Fischer, P., Marra, M., Ameling, C. & Cassee, F.R., 2013. Short-term effects of $PM_{2.5}$, PM_{10} and $PM_{2.5-10}$ on daily mortality in The Netherlands. *Science of the Total Environment*, 463-464, 20-6.

Juarez, E.K. & Petersen, M.R., 2021. A Comparison of Machine Learning Methods to Forecast Tropospheric Ozone Levels in Delhi. *Atmosphere*, 13.

Kafi, F., Yousefi, E., & Jahanishakib, F., 2023. Evaluation of Landscape Dynamics in City Thermal Islands

(Case Study: City of Birjand, Iran). *Environmental Energy and Economic Research*, 7(1), 1-25.

Lingxia, W., Qijie, Z., Jie, L. & Junlin, A., 2023. Hybrid machine learning model for hourly ozone concentrations prediction and exposure risk assessment. *Atmospheric Pollution Research*, 14, 101916.

Maji, K.J., Li, V.O. & Lam, J.C., 2020. Effects of China's current air pollution prevention and control action Plan on air pollution patterns, health risks and mortalities in Beijing 2014–2018. *Chemosphere*, 260, 127572.

Ou, J., Huang, Z., Klimont, Z., Jia, G., Zhang, S., Li, C., Meng, J., Mi, Z., Zheng, H. & Shan, Y., et al., 2020. Role of export industries on ozone pollution and its precursors in China. *Nature Communications*, 11(1), 1–12.

Pan, Q., Harrou, F. & Sun, Y., 2023. A comparison of machine learning methods for ozone pollution prediction. *Journal of Big Data*, 10.

Park, J., Shin, M., Lee, J. & Lee, J., 2021. Estimating the effectiveness of vehicle emission regulations for reducing NOx from light-duty vehicles in Korea using on-road measurements. *Science of the Total Environment*, 767, 144250.

Quesada-Ruiz, S., Attie, J.L., Lahoz, W.A., Abida, R., Ricaud, Ph., El Amraoui, L., Zbinden, R., Raespoor, K. & Asakereh, H., 2019. Satellite monitoring of ozone layer changes in Iran's atmosphere. *Natural Environment Hazards*, 8, 213-228.

Saxena, P. & Naik, V., 2019. Air pollution: sources, impacts and controls. CAB International. 215p.

Shami, S., Khush lahjeh Azar, M., Gorbani, Z., Moghimi, A., Mohamadzadeh, A., Sabet ghadam, S.S., 2021. Investigating the amount of changes in air pollutants during the spread of the Covid-19 virus in Iran using Sentinel 5 satellite data. *Scientific Journal of Mapping Sciences and Techniques*, 10, 135-146.

Su, X., An, J., Zhang, Y., Zhu, P., Zhu, B., 2020. Prediction of ozone hourly concentrations by support vector machine and kernel extreme learning machine using wavelet transformation and partial least squares methods. *Atmospheric Pollution Research*, 11(6), 51–60.

Theys, N. De Smedt, I., Yu, H., Danckaert, T., van Gent, J., Hormann, C., Wagner, T., Hedelt, P., Bauer, H., Romahn, F., Pedergnana, M., Loyola, D. & Van Roozendael, M., 2016. Sulfur dioxide retrievals from TROPOMI onboard Sentinel-5 Precursor: Algorithm Theoretical Basis. *Atmospheric Measurement Techniques*, 1-79.

Tiwari, S., Srivastava, A.K., Singh, A.K. & Singh, S., 2015. Identification of aerosol types over Indo-Gangetic Basin: implications to optical properties and associated radiative forcing. *Environmental Science and Pollution Research*, 22, 12246-60.

Van Wijk, J.J. & Van Selow, E.R., 1999. Cluster and calendar-based visualization of time series data, Proceedings 1999 IEEE Symposium on Information Visualization (InfoVis' 99). IEEE, pp. 4-9.

Vicente, D.J., Salazar, F., Lopez-Chacon, S.R., Soriano, C. & Martin-Vide, J., 2024. Evaluation of different machine learning approaches for predicting high concentration episodes of ground-level ozone: A case study in Catalonia, Spain. *Atmospheric Pollution Research*.

Wang, T., Xue, L., Brimblecombe, P., Lam, Y.F., Li, L., Zhang, L., 2017. Ozone pollution in China: a review of concentrations, meteorological influences, chemical precursors, and effects. *Science of the Total Environment*, 575, 1582–1596.

Wang, W., Liu, X., Bi, J. & Liu, Y., 2022. A machine learning model to estimate ground-level ozone concentrations in California using TROPOMI data and high-resolution meteorology. *Environment International*, 158, 106917.

Wang, W.N., Cheng, T.H., Gu, X.F., Chen, H., Guo, H., Wang, Y., Bao, F.W., Shi, S.Y., Xu, B.R., Zuo, X., et al., 2017. Assessing spatial and temporal patterns of observed ground-level ozone in China. *Scientific Reports*, 7(1), 1–12.

Wilkinson, L. & Friendly, M., 2009. The History of the Cluster Heat Map. *The American Statistician*, 63, 179-184.

Xian, G.Z., 2015. Remote sensing applications for the urban environment. CRC Press. 234p.

Xiong, Q., Wang, W., Wang, M., Zhang, C., Zhang, X., Chen, C. & Wang, M., 2022. Prediction of ground-level ozone by SOM-NARX hybrid neural network based on the correlation of predictors. iScience, 25, 105658.

Yousefi, E., Sayadi, M., & Chamenhpour, E., 2022. Google Earth Engine platform to calculate the hydrometeorology and hydrological water balance of wetlands in arid areas and predict future changes. *Journal of Applied Research in Water and Wastewater*, *9*(1), 52-68.

Zhao, F., Liu, C., Cai, Z., Liu, X., Bak, J., Kim, J., Hu, Q., Xia, C., Zhang, C., Sun, Y., Wang, W. & Liu, J., 2021. Ozone profile retrievals from TROPOMI: Implication for the variation of tropospheric ozone during the outbreak of COVID-19 in China. *Science of the Total Environment*, 764, 142886.

Zhao, S., Guo, Y., Sheng, Q. & Shyr, Y., 2014. Advanced heat map and clustering analysis using heatmap3. *BioMed Research International*, 2014, 986048.